Spinning σ-model Solitons in 2 + 1 Anti-de Sitter Space

A. Stern – University of Alabama

B. Harms – University of Alabama

Citation of published version:

Harms, B., Stern, A. (2016): Spinning σ-model Solitons in 2 + 1 Anti-de Sitter Space. *Physics Letters B*, 763(Pages 401-408).
DOI: https://doi.org/10.1016/j.physletb.2016.10.075

Physics Letters B 763 (2016) 401–408

Contents lists available at ScienceDirect

Physics Letters B

www.elsevier.com/locate/physletb

Spinning σ-model solitons in $2+1$ anti-de Sitter space

B. Harms, A. Stern *

Department of Physics, University of Alabama, Tuscaloosa, AL 35487, USA

ARTICLE INFO

Article history:
Received 6 October 2016
Accepted 14 October 2016
Available online 4 November 2016
Editor: M. Cvetič

ABSTRACT

We obtain numerical solutions for rotating topological solitons of the nonlinear σ-model in three-dimensional anti-de Sitter space. Two types of solutions, *i*) and *ii*), are found. The σ-model fields are everywhere well defined for both types of solutions, but they differ in their space–time domains. Any time slice of the space–time for the type *i*) solution has a causal singularity, despite the fact that all scalars constructed from the curvature tensor are bounded functions. No evidence of a horizon is seen for any of the solutions, and therefore the type *i*) solutions have naked singularities. On the other hand, the space–time domain, along with the fields, for the type *ii*) solutions are singularity free. Multiple families of solutions exhibiting bifurcation phenomena are found for this case.

1. Introduction

Asymptotically AdS solutions are of current interest due to their application to holography and their indication of possible phase transitions in the boundary field theory [1]. Examples of such solutions are AdS black holes [2], AdS solitons [3], and their hairy extensions [4–7]. Here we show the existence of asymptotically AdS^3 σ-model solitons. Their stability requires the fields to be rotating. Nonrotating asymptotically AdS^3 σ-model solitons were previously shown not to exist [8]. This is also evident from a simple scaling argument. While the σ-model Lagrangian in two spatial dimensions is scale invariant for static field configurations, this is no longer the case in a background anti-de Sitter space. Rather, there is a contribution which scales like r^2, leading to an attractive force, in addition to the gravitational attraction. The absence of any stabilizing forces, is thus consistent with the nonexistence of static solutions. The above arguments do not apply for rotating field configurations. We show that, as a result, there exist rotating topological solitons which approach AdS^3 in the large distance limit. Asymptotically flat self-gravitating solitons in the $2+1$ dimensional nonlinear σ-models have been known to exist for a long time [9]. Analogous self-gravitating solutions, or skyrmions, in $3+1$ dimensions are well known [10]. Spinning skyrmions in $3+1$ dimensional gravity have also been considered [11]. Solutions with large winding number (corresponding to baryon number) have been proposed to model dense stars [12–14]. Singularities and horizons can arise for skyrmions in space–times with different cosmological constants. Such solutions are hairy black holes, and they have been extensively studied [10,15–28] It is of interest to know if the $2+1$ dimensional nonlinear σ-model also admits solutions with horizons at finite distances.

Here we examine the standard nonlinear σ-model coupled to gravity with a negative cosmological constant. Our ansatz for σ-model fields in $2+1$ dimensions is suitable for the construction of solitons with arbitrary winding number. Using numerical methods we obtain two types of rotating soliton solutions with integer winding number. This is due to the existence of two types of space–time metrics near the origin. From either space–time metric one gets that all scalars constructed from the curvature tensor are bounded at the origin. Nevertheless, the origin is a casual singularity for one case, which we denote by *i*) and not the other, which we denote by *ii*). The singularity for the type *i*) solution closely resembles that of a BTZ black hole. Here it is a naked singularity because the solutions have no horizons.[1] The σ-model fields are everywhere well defined for solitons *i*), even though the domain has a singularity, i.e., the fields have a well-defined limit at the casual singularity. Thus the solitons *i*) are restricted to distinct topological sectors, and they are thus topological solitons. There are no space–time singularities (or horizons) for solutions *ii*), and they too are topological solitons. From their asymptotic form at

* Corresponding author.
E-mail addresses: bharms@ua.edu (B. Harms), astern@ua.edu (A. Stern).

[1] Solutions with singular metric tensors are of physical relevance in $2+1$ gravity. Examples of singularities are the helical and conical singularities appearing in the metric tensor of point particles with, and without spin, respectively. As with our type i) solutions, all scalar quantities constructed from the associated curvature tensor are bounded everywhere. Furthermore, since our type i), as well as the type ii) solutions, are asymptotically AdS, they are of interest for the AdS/CFT correspondence.

http://dx.doi.org/10.1016/j.physletb.2016.10.075

spatial infinity, the types *i*) and *ii*) solitons can be labeled by the same parameters as is used to label a BTZ black hole, namely, mass and angular momentum, with the addition of parameters associated with the matter content. An alternative mass and angular momentum can be assigned to the solitons using collective coordinate techniques. Collective coordinate quantization leads to the usual spectrum for a rigid rotor in two spatial dimensions.

We denote the nonlinear σ-model fields by Φ_a, $a = 1, 2, 3$, constrained on S^2, $\Phi_a \Phi_a = 1$. The action for Φ_a coupled to $2+1$ gravity is

$$S = \int d^3x \sqrt{-g} \Big(\frac{1}{16\pi G}(R - 2\Lambda) - \frac{1}{2}\partial_\mu \Phi_a \partial^\mu \Phi_a + \lambda(\Phi_a \Phi_a - 1) \Big) + S_{GHY} - S_{AdS} \,, \tag{1}$$

where G is the three-dimensional version of Newton's constant (here in dimensionless units), Λ is the cosmological constant, and λ is a Lagrange multiplier. S_{GHY} is the Gibbons–Hawking–York term [29] on the boundary at spatial infinity $r \to \infty$,

$$S_{GHY} = \frac{1}{8\pi G} \int\limits_{r\to\infty} d^2x \sqrt{-h}\, K \,. \tag{2}$$

h is the determinant of the induced metric on the boundary, and K is the trace of the extrinsic curvature, $K = -\frac{1}{\sqrt{-g}} \partial_\mu (\sqrt{-g}\, \hat{n}^\mu)$, where $\hat{n}_\mu$ is the unit vector normal to the boundary. S_{AdS} is the infinite AdS vacuum action, which we subtract off in order for the gravity contribution to the action to be finite. Just as in flat space-time, one needs that $\Phi_a \to$ constant as $r \to \infty$, in order for the matter contribution to the action to be finite. This identification implies that the domain for the nonlinear-sigma model on any time-slice is S^2, and topologically distinct field configurations result. We demand that Φ_a has a unique limit everywhere on S^2, including at the point associated with the origin, which may or may not be a causal singularity. We label the topological sectors by the winding number

$$n = -\frac{1}{8\pi} \int\limits_{x^0 = \text{constant}} d^2x\, \epsilon_{abc} \epsilon_{ij} \Phi_a \partial_i \Phi_b \partial_j \Phi_c \,, \tag{3}$$

where the integral is on any time-slice, and n is normalized to be an integer. ϵ_{abc} and ϵ_{ij} denote totally antisymmetric tensors, and $i, j, .. = 1, 2$ are spatial indices.

In section 2 we write down the ansatz for the metric tensor and Φ_a and give asymptotic solutions near spatial infinity and the origin. Some numerical solutions are presented in section 3. Collective coordinate quantization is shown in section 4. The question of the existence of black hole solutions with nonlinear σ-model hair is examined in section 5, while some brief concluding remarks are given in section 6.

2. Asymptotic solutions

We parametrize any two-dimensional time-slice with polar coordinates (r, ϕ), and the time by t. Our ansatz for the metric tensor is expressed in terms of three radial functions A, B and Ω,

$$ds^2 = -A(r) dt^2 + \frac{B(r)}{A(r)} dr^2 + r^2 \Big(d\phi + \Omega(r) dt \Big)^2 \,, \tag{4}$$

while the σ-model fields Φ_a are written in terms of one radial function χ and a fixed angular velocity ω,

$$\begin{pmatrix} \Phi_1 \\ \Phi_2 \\ \Phi_3 \end{pmatrix} = \begin{pmatrix} \sin\chi(r)\, \cos(\phi - \omega t) \\ \sin\chi(r)\, \sin(\phi - \omega t) \\ \cos\chi(r) \end{pmatrix} \,. \tag{5}$$

The functions A, B and χ are dimensionless, while Ω and ω have units of inverse-time. Without any loss of generality we can set $\chi(\infty) = 0$. Then for fields in the n^{th} topological sector, $\chi(0) = n\pi$. Upon substituting (4) and (5) into the action (including the Gibbons–Hawking–York term) we get

$$S = \frac{\pi}{\kappa} \int \frac{dtdr}{\sqrt{B}} \Big\{ \partial_r A + \frac{r^3 (\partial_r \Omega)^2}{2} + \frac{2rB}{\ell^2} - r\kappa \Big(A(\partial_r \chi)^2 + \Big(\frac{1}{r^2} - \frac{(\omega + \Omega)^2}{A} \Big) B \sin^2\chi \Big) \Big\} - S_{AdS} \,, \tag{6}$$

where $\kappa = 8\pi G$, and we set $\Lambda = -\frac{1}{\ell^2}$. It is convenient to introduce the dimensionless radial variable $x = r/\ell$. Then

$$S = \frac{\pi}{\kappa} \int \frac{dtdx}{\sqrt{B}} \Big\{ A' + \frac{x^3 \tilde{\Omega}'^2}{2} + 2xB - x\kappa \Big(A\chi'^2 + \Big(\frac{1}{x^2} - \frac{(\tilde{\omega} + \tilde{\Omega})^2}{A} \Big) B \sin^2\chi \Big) \Big\} - S_{AdS} \,, \tag{7}$$

where $\tilde{\Omega} = \ell\,\Omega$ and $\tilde{\omega} = \ell\,\omega$, and the prime denotes a derivative with respect to x. Upon extremizing the action with respect to variations in A, B, $\tilde{\Omega}$ and χ, we get

$$\begin{aligned} \frac{1}{2}(\ln B)' &= \kappa x \Big(\chi'^2 + \frac{B}{A^2} (\tilde{\omega} + \tilde{\Omega})^2 \sin^2\chi \Big) \\ 0 &= A' + \frac{x^3 \tilde{\Omega}'^2}{2} - 2xB + \kappa x \Big(-A\chi'^2 + \Big(\frac{1}{x^2} - \frac{(\tilde{\omega} + \tilde{\Omega})^2}{A} \Big) B \sin^2\chi \Big) \\ \Big(\frac{x^3 \tilde{\Omega}'}{\sqrt{B}} \Big)' &= \frac{2\kappa x}{A} \sqrt{B}\, (\tilde{\Omega} + \tilde{\omega})\, \sin^2\chi \\ \Big(\frac{xA\chi'}{\sqrt{B}} \Big)' &= x\sqrt{B} \Big(\frac{1}{x^2} - \frac{(\tilde{\omega} + \tilde{\Omega})^2}{A} \Big) \sin\chi\, \cos\chi \,, \end{aligned} \tag{8}$$

respectively.

Next we write down the solutions to (8) in the asymptotic regions $x \to \infty$ and $x \to 0$.

2.1. $x \to \infty$

For the asymptotic region $x \to \infty$ we demand that $\chi \to 0$ and that we recover anti-de Sitter space in the limit. The large distance behavior for A, B, $\tilde{\Omega}$ and χ can be determined from (8):

$$\begin{aligned} A &\to x^2 - M + \frac{J^2}{x^2} + \frac{\kappa\nu^2 \Big(\big(\tilde{\Omega}_\infty + \tilde{\omega} \big)^2 + 4M + 1 \Big)}{12x^4} + \mathcal{O}\Big(\frac{1}{x^6} \Big) \\ B &\to 1 - \frac{2\kappa\nu^2}{x^4} + \frac{\kappa\nu^2 \Big(\big(\tilde{\Omega}_\infty + \tilde{\omega} \big)^2 - 8M - 2 \Big)}{3x^6} + \mathcal{O}\Big(\frac{1}{x^8} \Big) \\ \tilde{\Omega} &\to \tilde{\Omega}_\infty + \frac{J}{x^2} + \frac{\kappa\nu^2 \big(\tilde{\Omega}_\infty + \tilde{\omega} - 4J \big)}{12\,x^6} + \mathcal{O}\Big(\frac{1}{x^8} \Big) \\ \chi &\to \frac{\nu}{x^2} + \frac{\nu \Big(-\big(\tilde{\Omega}_\infty + \tilde{\omega} \big)^2 + 4M + 1 \Big)}{8\,x^4} + \mathcal{O}\Big(\frac{1}{x^6} \Big) \,, \\ & \qquad x \to \infty \,, \end{aligned} \tag{9}$$

where M, J, $\tilde{\Omega}_\infty$ and ν are constants, the first two being the mass and angular momentum parameters, respectively. The solution is

consistent with the standard large distance behavior of the metric tensor for three-dimensional anti-de Sitter space with a localized matter source [4]. The Ricci scalar tends towards the AdS^3 value of -6 in the limit. The constant $\tilde{\Omega}_\infty$ can always be eliminated by transforming to the co-rotating frame at spatial infinity, where $\tilde{\omega}$ in the ansatz (5) gets replaced by $\tilde{\Omega}_\infty + \tilde{\omega}$. Conversely, we can transform to a frame where the σ-model fields are static by replacing $\tilde{\Omega}_\infty$ by $\tilde{\Omega}_\infty + \tilde{\omega}$.

2.2. $x \to 0$

Two possible power series expansions for A, B, $\tilde{\Omega}$ and χ exist near the origin. Two of the functions, A and $\tilde{\Omega}$, are singular at the origin for one solution, while all functions have a finite limit for the other. For the former, $A, \tilde{\Omega} \sim \frac{1}{x^2}$, as $x \to 0$. More specifically, near the origin the solution has the form

$$
\begin{aligned}
A &\to \frac{{J_0}^2}{x^2} - M_0 + B_0 x^2 - \frac{\kappa}{3} M_0 \chi_2^2 x^4 + \mathcal{O}(x^6) \\
B &\to B_0 \left(1 + 2\kappa \chi_2^2 x^4 + \frac{\kappa \chi_2^2}{3 {J_0}^2}(B_0 + 8M_0) x^6 + \mathcal{O}(x^8)\right) \\
\tilde{\Omega} &\to \frac{J_0}{x^2} + \tilde{\Omega}_0 - \kappa J_0 \chi_2^2 x^2 - \frac{2\kappa M_0 \chi_2^2}{3 J_0} x^4 + \mathcal{O}(x^6) \\
\chi &\to n\pi + \chi_2 x^2 + \frac{\chi_2 M_0}{2 {J_0}^2} x^4 + \mathcal{O}(x^6), \qquad x \to 0, \qquad (10)
\end{aligned}
$$

where J_0, M_0, B_0, $\tilde{\Omega}_0$ and χ_2 are constants. For finite $J_0 \neq 0$, M_0, B_0, $\tilde{\Omega}_0$, the time-time component $g_{tt} = -A + x^2 \tilde{\Omega}^2$, as well as the remaining components of the metric tensor, are bounded at the origin,

$$
ds^2 \sim (M_0 + 2 J_0 \tilde{\Omega}_0)\, dt^2 + \frac{B_0}{J_0^2} x^2\, dx^2 + 2 J_0\, dt d\phi + x^2\, d\phi^2 . \qquad (11)
$$

All scalars constructed from the curvature tensor are bounded in the $x \to 0$ limit, e.g. the Ricci scalar tends toward $\frac{4\kappa {J_0}^2 \chi_2^2}{B_0} - 6$. Nevertheless, a causal singularity exists at the origin for this solution. The metric tensor near the origin closely resembles that of the BTZ black hole [2]. For the numerical solutions discussed in section 3 there are no horizons at finite x, and so the singularity is naked for all such solutions.

The power series solution (11) is not valid for $J_0 = 0$. For this case one has the alternative power series solution

$$
\begin{aligned}
A &\to -M_0 - M_0 x^2 + \frac{\kappa}{8} \chi_1^2 \left(-3M_0 + (\tilde{\Omega}_0 + \tilde{\omega})^2\right) x^4 + \mathcal{O}(x^6) \\
B &\to -M_0 - \kappa M_0 \chi_1^2 x^2 + \frac{\kappa}{8} \chi_1^2 \Big(-M_0 \left(2\chi_1^2 (5\kappa - 1) - 9\right) \\
&\quad + (\tilde{\Omega}_0 + \tilde{\omega})^2\Big) x^4 + \mathcal{O}(x^6) \\
\tilde{\Omega} &\to \tilde{\Omega}_0 + \frac{\kappa}{4} \chi_1^2 (\tilde{\Omega}_0 + \tilde{\omega}) x^2 \\
&\quad - \frac{\kappa}{48 M_0} \chi_1^2 (\tilde{\Omega}_0 + \tilde{\omega}) \Big(-M_0 \left(2\chi_1^2 (4\kappa - 1) - 7\right) \\
&\quad - (\tilde{\Omega}_0 + \tilde{\omega})^2\Big) x^4 + \mathcal{O}(x^6) \\
\chi &\to n\pi + \chi_1 x - \frac{\chi_1}{24 M_0} \Big(-M_0 \left(2\chi_1^2 (3\kappa - 1) - 9\right) \\
&\quad - 3(\tilde{\Omega}_0 + \tilde{\omega})^2\Big) x^3 + \mathcal{O}(x^5), \qquad x \to 0, \qquad (12)
\end{aligned}
$$

where all functions have a finite limit. This solution is parametrized by M_0, $\tilde{\Omega}_0$ and χ_1. The invariant length near the origin takes the form

$$
ds^2 \sim M_0 (1 + x^2) dt^2 + \left(1 + (\kappa \chi_1^2 - 1) x^2\right) dx^2 + x^2 (d\phi + \tilde{\Omega}_0 dt)^2 . \qquad (13)
$$

For a Lorentzian space–time near the origin we need that $M_0 < 0$. When $\tilde{\Omega}_0 = 0$, any t-slice approaches flat Euclidean space as $x \to 0$. When $\tilde{\Omega}_0 \neq 0$, the space–time near the origin is rotating. In either case, the space–time is singularity free.

3. Numerical solutions

We have not found any analytic solutions to (8) away from the asymptotic regions and therefore rely on numerical methods. We numerically integrate (8) subject to the asymptotic expressions (9) near the AdS^3 boundary to obtain A, B, $\tilde{\Omega}$ and χ at finite x. For topological solitons $\chi(0)$ must be an integer multiple of π. The topological solitons solutions can be parametrized by the constants J, M, ν and $\tilde{\Omega}_\infty$ appearing in (9). One strategy for obtaining solutions is to first fix three of the parameters (along with κ and $\tilde{\omega}$), and then apply shooting methods to tune the remaining one such that $\chi \to n\pi$ as $x \to 0$, where the winding number n is equal to a nonzero integer. Near the origin the solutions must satisfy either (10) or (12), corresponding to type i) or ii) solutions, respectively. The parameters appearing in (10) or (12) can then be determined numerically from M, J, ν and $\tilde{\Omega}_\infty$. Conversely, given J_0, M_0, B_0, $\tilde{\Omega}_0$ and χ_2 of the expression (10) or M_0, $\tilde{\Omega}_0$ and χ_1 of (12) (and the winding number n) we can numerically determine the parameters M, J, ν and $\tilde{\Omega}_\infty$ describing the large distance behavior.

3.1. Type i) solutions

Numerical solutions satisfying (10) near the origin corresponding to type i) solutions are found for large regions of the parameter space. Examples of the behavior of the functions $A(x)$ and $\chi(x)$ for these solutions appear in figures 1 through 5. There we plot χ versus $\log(x)$ and $\log(A)$ versus $\log(x)$ for different values of n, $\tilde{\omega}$, M, J and κ. We set $\tilde{\Omega}_\infty = 0$, which means that we are working in the co-rotating frame as $x \to \infty$. In the captions we list the fitted values for ν for each solution. One example which appears in all Figures 1–5 is the $n = 1$ soliton with $\kappa = \tilde{\omega} = M = J = 1$ and $\nu \approx 2.33$. For this example the functions A, B, $\tilde{\Omega}$ and χ tend towards (10) as $x \to 0$, with the following values for the short distance parameters: $M_0 \sim -.34$, $J_0 \sim .094$, $B_0 \sim .0035$, $\tilde{\Omega}_0 \sim 1.92$ and $\chi_2 \sim -14.9$.

Solutions i) with winding number one, two and three, with $M = J = \kappa = \tilde{\omega} = 1$, are shown in Figs. 1a and 1b. $n = 1$ solutions are plotted for different rotation velocities $\tilde{\omega}$, including zero, (with $M = J = \kappa = 1$) in Figs. 2a and 2b. $n = 1$ solutions are plotted for different values of the mass parameter, including 0 and -1, (with $J = \kappa = \tilde{\omega} = 1$) in Figs. 3a and 3b and different values of the angular momentum parameter, including 0, (with $M = \kappa = \tilde{\omega} = 1$) in Figs. 4a and 4b. Finally, $n = 1$ solutions are plotted in Figs. 5a and 5b for different values of κ (with $M = J = \tilde{\omega} = 1$). From the results in Figs. 2 and 4, neither a nonzero rotation velocity $\tilde{\omega}$ in the internal space nor a nonzero angular momentum J is necessary to stabilize the soliton, since we find solutions when either $\tilde{\omega}$ is zero or J is zero. On the other hand, we find no solutions when both $\tilde{\omega}$ and J vanish, which is consistent with the no-go result in [8]. In addition, we find novel solutions where both the mass and angular momentum parameters vanish, $M = J = 0$, and one with $M = -1$, $J = 0$. If one takes these as parameters for the BTZ black hole, the former would correspond to a zero mass black hole and

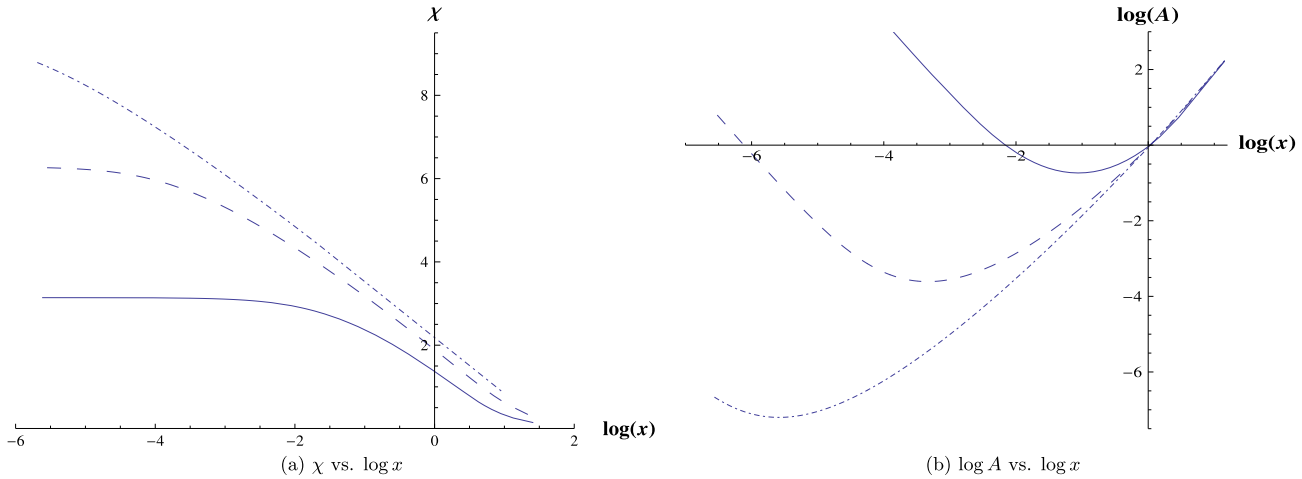

(a) χ vs. $\log x$ (b) $\log A$ vs. $\log x$

Fig. 1. Varying n. Self-gravitating rotating solitons with parameters: $M = J = \kappa = \tilde{\omega} = 1$. χ versus $\log x$ is plotted in figure (a), and $\log A$ versus $\log x$ is plotted in figure (b). $\nu \approx 2.33$ gives the $n = 1$ soliton (solid curve), $\nu \approx 4.92$ gives the $n = 2$ soliton (dashed curve) and $\nu \approx 7.52$ gives the $n = 3$ soliton (dot-dashed curve).

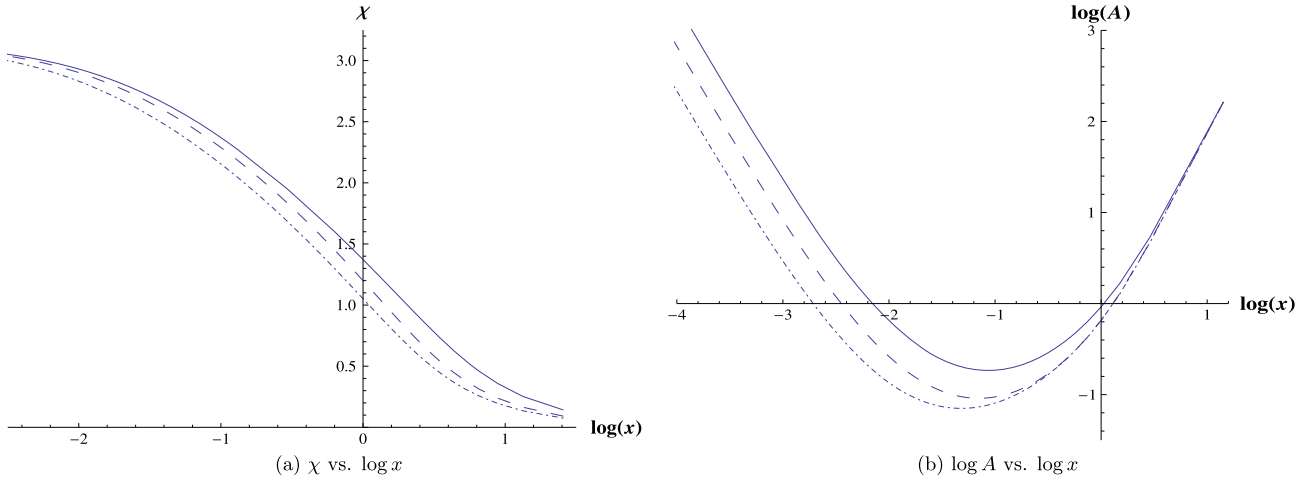

(a) χ vs. $\log x$ (b) $\log A$ vs. $\log x$

Fig. 2. Varying $\tilde{\omega}$. $n = 1$ self-gravitating solitons with parameters: $M = J = \kappa = 1$ for different values of $\tilde{\omega}$. χ versus $\log x$ is plotted in figure (a), and $\log A$ versus $\log x$ is plotted in figure (b). $\nu \approx 2.33$ gives the soliton with $\tilde{\omega} = 1$ (solid curve), $\nu \approx 1.48$ gives the soliton with $\tilde{\omega} = 0$ (dashed curve) and $\nu \approx 1.22$ gives the soliton with $\tilde{\omega} = -1$ (dot-dashed curve).

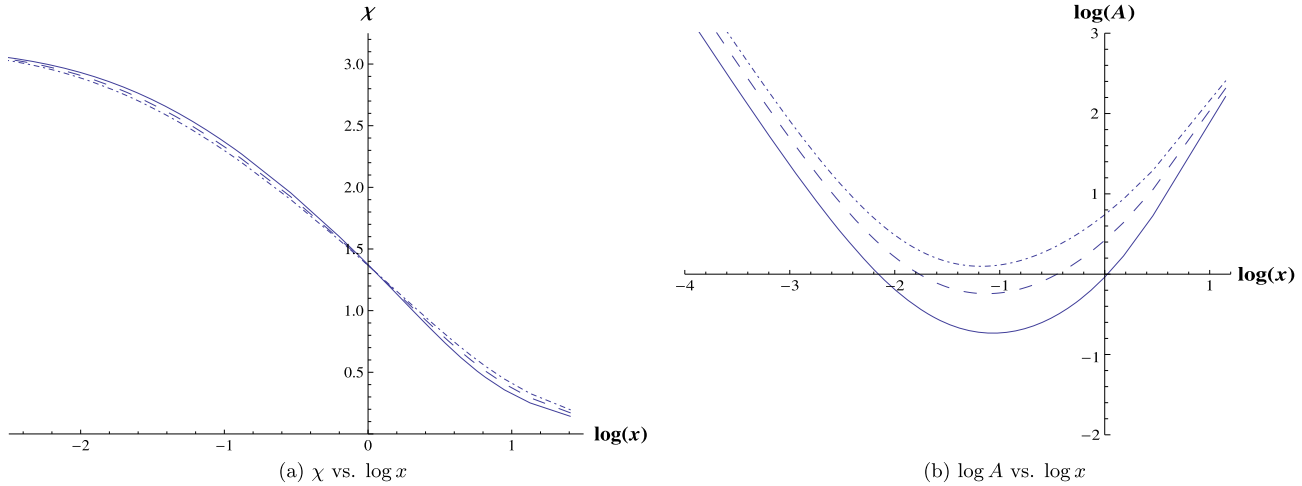

(a) χ vs. $\log x$ (b) $\log A$ vs. $\log x$

Fig. 3. Varying M. $n = 1$ self-gravitating solitons with parameters: $J = \kappa = \tilde{\omega} = 1$ for different values of the mass parameter M. χ versus $\log x$ is plotted in figure (a), and $\log A$ versus $\log x$ is plotted in figure (b). $\nu \approx 2.33$ gives the soliton with $M = 1$ (solid curve), $\nu \approx 2.89$ gives the soliton with $M = 0$ (dashed curve) and $\nu \approx 3.42$ gives the soliton with $M = -1$ (dot-dashed curve).

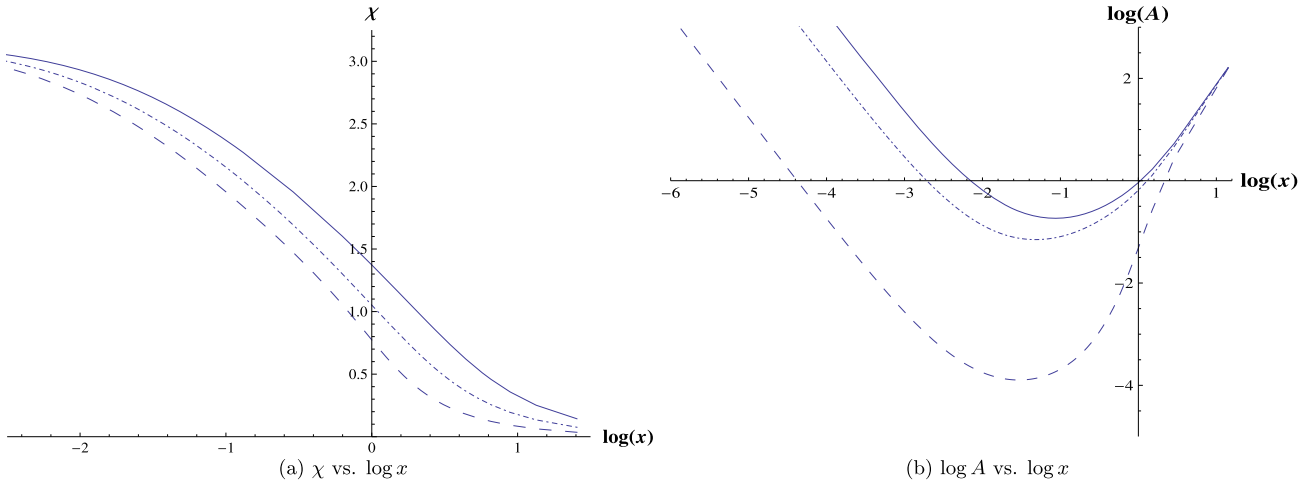

(a) χ vs. $\log x$ (b) $\log A$ vs. $\log x$

Fig. 4. Varying J. $n = 1$ self-gravitating solitons with parameters: $M = \kappa = \tilde{\omega} = 1$ for different values of the angular momentum parameter J. χ versus $\log x$ is plotted in figure (a), and $\log A$ versus $\log x$ is plotted in figure (b). $\nu \approx 2.33$ gives the soliton with $J = 1$ (solid curve), $\nu \approx .569$ gives the soliton with $J = 0$ (dashed curve) and $\nu \approx 1.22$ gives the soliton with $J = -1$ (dot-dashed curve).

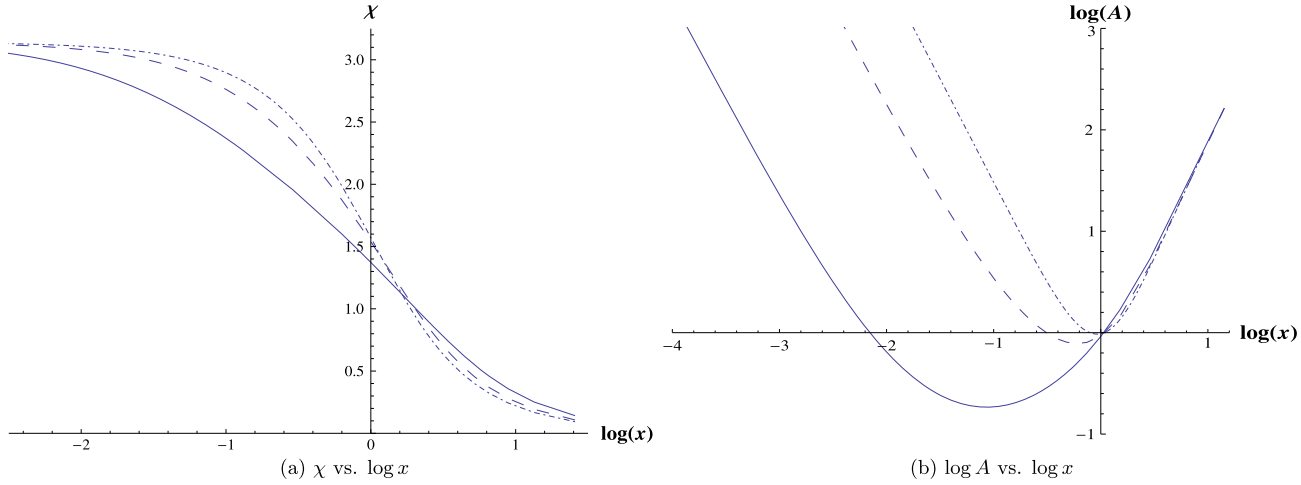

(a) χ vs. $\log x$ (b) $\log A$ vs. $\log x$

Fig. 5. Varying κ. $n = 1$ self-gravitating solitons with parameters: $M = J = \tilde{\omega} = 1$ for different values of κ. χ versus $\log x$ is plotted in figure (a), and $\log A$ versus $\log x$ is plotted in figure (b). $\nu \approx 2.33$ gives the soliton with $\kappa = 1$ (solid curve), $\nu \approx 1.76$ gives the soliton with $\kappa = .25$ (dashed curve) and $\nu \approx 1.52$ gives the soliton with $\kappa = .05$ (dot-dashed curve).

the latter would correspond to anti-de Sitter space. An example of a soliton with $M = J = 0$ occurs for $\kappa = \tilde{\omega} = 1$, $\nu \approx .77$, and a soliton with $M = -1$, $J = 0$ occurs for $\kappa = \tilde{\omega} = 1$, $\nu \approx 1.061$. As required, A approaches x^2 as $x \to \infty$ for all of the above examples, while it does not pass through zero for any x. The latter behavior indicates that there are no horizons. A and Ω go as $1/x^2$ near the origin.

3.2. *Type ii) solutions*

Numerical solutions can also be found for which all of the functions are bounded, including at the origin where they approach (12). These solutions cover a smaller region in parameter space than *i*) since they correspond to the limiting case of $J_0 \to 0$ in (11). By integrating from $x \to \infty$ using (9) and from $x \to 0$ using (12) we can match the four functions A, B, Ω and χ, along with their derivatives, at finite x to arbitrary accuracy. An example of such a solution is shown in Fig. 6(a), where $M_0 \approx -.193$, $\tilde{\Omega}_0 \approx -2.09$, $\chi_1 \approx -8.08$, $\omega \approx 1.37$ and $\kappa \approx .246$. All four functions are well behaved at the origin. By matching the functions and their derivatives at $x = 1$, we determined the parameters of the large distance solution (9) to be $M \approx .0539$, $J \approx .0817$, $\Omega_\infty \approx -2.77$ and $\nu \approx .241$. As in the previous figures, A does not cross the x-axis, indicating no horizons. The function $\chi(x)$ monotonically decreases from π to 0 as x goes from 0 to ∞. On the other hand, solutions can also be found where $\chi(x)$ has multiple nodes, as is illustrated in Fig. 6(b) for solutions with zero, one and two nodes. The depicted $n = 1$ solutions have common values for κ, ω and M_0, and differing values of the parameters χ_1 and $\tilde{\Omega}_0$.

The space of nonsingular solutions can be parametrized by ω, κ, M_0, $\tilde{\Omega}_0$ and χ_1. We examine the parameter space for the zero, one and two node solutions in Figs. 7, 8(a) and 8(b). Keeping κ and ω fixed, we plot $-\chi_1$ versus $\tilde{\Omega}_0$ in Fig. 7. $\chi_1(\tilde{\Omega}_0)$ is seen to be multi-valued, with a cusp singularity occurring for the zero node solutions at some minimum value of $\tilde{\Omega}_0$. (Analogous behavior has been noted for self-gravitating Skyrmions [16].) $-\chi_1(\kappa)$ [with ω and M_0 held fixed] is plotted in Fig. 8(a) and $-\chi_1(-M_0)$ [with ω and κ held fixed] is plotted in Fig. 8(b). Finite domains are seen for both of these functions, implying upper bounds on the allowed values for κ and $-M_0$. We also get no soliton solutions in the limiting cases of $\kappa \to 0$ and $-M_0 \to 0$. [The latter limit corresponds to the function A vanishing at the origin, indicating a horizon in the zero radius limit. If solutions existed with $-M_0 \to 0$ they could coincide with the zero radius limit of the horizon of a hairy black

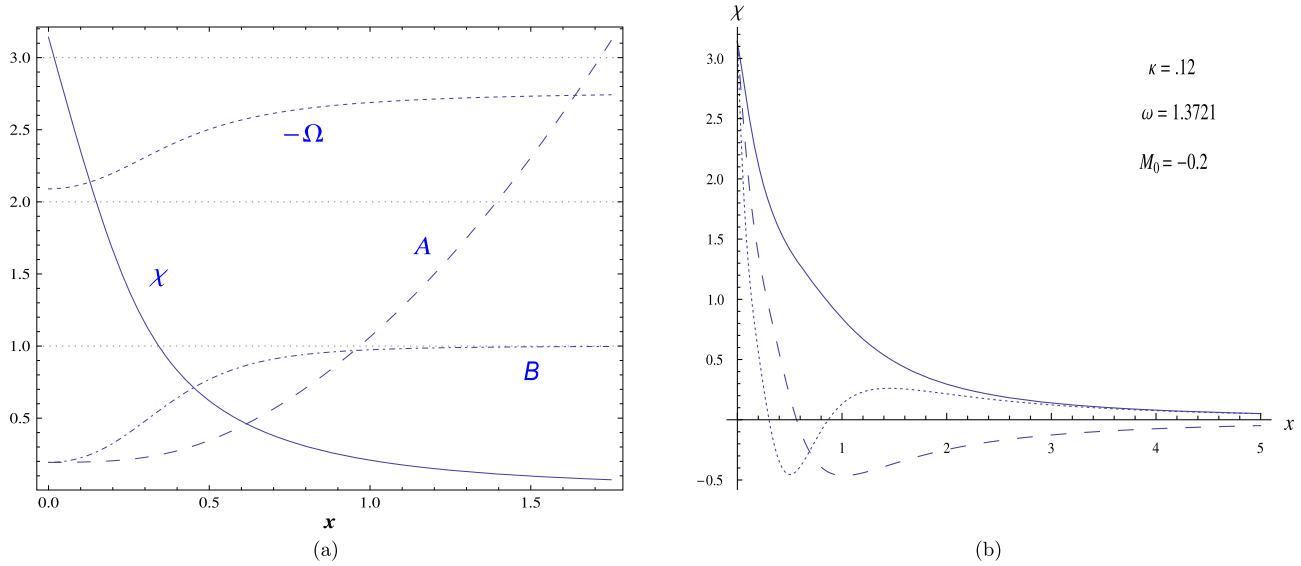

Fig. 6. Singularity-free solutions. In (a), χ (solid curve), A (large dashed curve), B (dot-dashed curve) and $-\tilde{\Omega}$ (small dashed curve) are plotted versus x for a singularity-free solution for the following values of the parameters introduced in (12): $M_0 \approx -.193$, $\tilde{\Omega}_0 \approx -2.09$, $\chi_1 \approx -8.08$, $\omega \approx 1.37$ and $\kappa \approx .246$. In (b), $\chi(x)$ is plotted for three different soliton solutions having $\kappa \approx .12$, $\omega \approx 1.3721$ and $M_0 \approx -.2$ The monotonically decreasing solution (solid curve) has $\chi_1 \approx -5.80$ and $\tilde{\Omega}_0 \approx -3.01$; The single node solution (dashed curve) has $\chi_1 \approx -11.94$ and $\tilde{\Omega}_0 \approx -3.52$; The double node solution (dotted curve) has $\chi_1 \approx -23.25$ and $\tilde{\Omega}_0 \approx -4.19$.

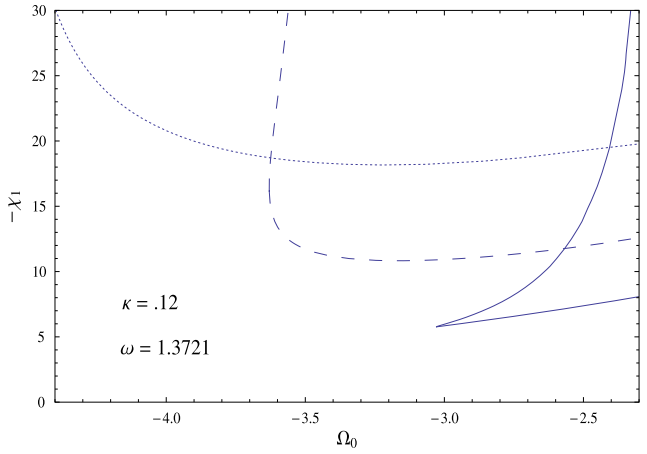

Fig. 7. $-\chi_1(\tilde{\Omega}_0)$ [with $\kappa = .12$ and $\omega = 1.3721$] is plotted for the solutions having monotonically decreasing χ (solid curve), the single node solutions (dashed curve) and the double node solutions (dotted curve). $\chi_1(\tilde{\Omega}_0)$ is seen to have a cusp singularity at $\tilde{\Omega}_0 \approx -3.02$ for the zero node solutions.

hole. The absence of such solutions is then consistent with not finding any black hole solutions with σ-model hair, which is what we report in section 5.]

4. Collective coordinate quantization

Collective coordinate quantization allows for an alternative definition of the mass and angular momentum of the soliton. We denote them by $\mathcal{M}$ and $\mathcal{J}$, respectively. Both can be computed from the action (1) evaluated for the soliton. A Chern–Simons term [30,31] can be included in the total action, and this will produce a contribution which is linear in the angular velocity, in addition to those coming from (1). However, such contributions do not affect the energy spectrum, and so we will not consider the Chern–Simons term.

In the collective coordinate approach one replaces $\tilde{\omega}$ with a dynamical angular velocity $\dot{\psi}$, with the caveat that its variation is sufficiently small so that it doesn't significantly change the values of the mass $\mathcal{M}$ or the moment of inertia $\mathcal{I}$ of the soliton. $\mathcal{M}$ is defined as the $\dot{\psi}$-independent contribution to the soliton action, while $\mathcal{I}/2$ is the coefficient of the quadratic contribution in $\dot{\psi}$. As indicated above, there is also a linear contribution. Thus the soliton action can be written

$$S = \int dt \left\{ \frac{1}{2}\mathcal{I}\dot{\psi}^2 + \alpha\dot{\psi} - \mathcal{M} \right\}, \tag{14}$$

where $\mathcal{I}$, α and $\mathcal{M}$ are given by the radial integrals

$$\begin{aligned}
\mathcal{I} &= 2\pi \int dx \frac{x\sqrt{B}}{A} \sin^2\chi \\
\alpha &= 2\pi \int dx \frac{x\tilde{\Omega}\sqrt{B}}{A} \sin^2\chi \\
\mathcal{M} &= -\frac{\pi}{\kappa} \int \frac{dx}{\sqrt{B}} \left\{ A' + \frac{x^3\tilde{\Omega}'^2}{2} + 2xB \right. \\
&\qquad \left. - x\kappa \left(A\chi'^2 + \left(\frac{1}{x^2} - \frac{\tilde{\Omega}^2}{A} \right) B \sin^2\chi \right) - 4x\sqrt{B} \right\}.
\end{aligned} \tag{15}$$

The infinite AdS vacuum action S_{AdS} was subtracted from $\mathcal{M}$. The angular momentum of the soliton is $\mathcal{J} = \mathcal{I}\dot{\psi}$. From the asymptotic behavior (9) as $x \to \infty$ and the behavior (10) or (12) as $x \to 0$, the integral expressions for $\mathcal{I}$, α and $\mathcal{M}$ are finite. (This is in contrast to the moment of inertia for the σ-model soliton in Minkowski space–time, which is not bounded, leading to a spontaneous breakdown of rotational symmetry [32].) For the $n = 1$ solution with $M = J = 1$ appearing in figures 1 through 5 we get $\mathcal{M} \approx -22.1$ and $\mathcal{J} = \mathcal{I}\tilde{\omega} \approx 7.6$. For the topological soliton illustrated in Fig. 6 having $M \approx .0539$ and $J \approx .0817$ we get $\mathcal{M} \approx 2.1$ and $\mathcal{J} = \mathcal{I}\tilde{\omega} \approx 2.78$.

The Hamiltonian for the system is

$$H = \frac{\mathcal{J}^2}{2\mathcal{I}} + \mathcal{M}\,. \tag{16}$$

The angular momentum $\mathcal{J}$ is related to the canonical momentum p_ψ by $\mathcal{J} = p_\psi - \alpha$. Its Poisson bracket with the $U(1)$ phase $e^{i\psi}$ is then

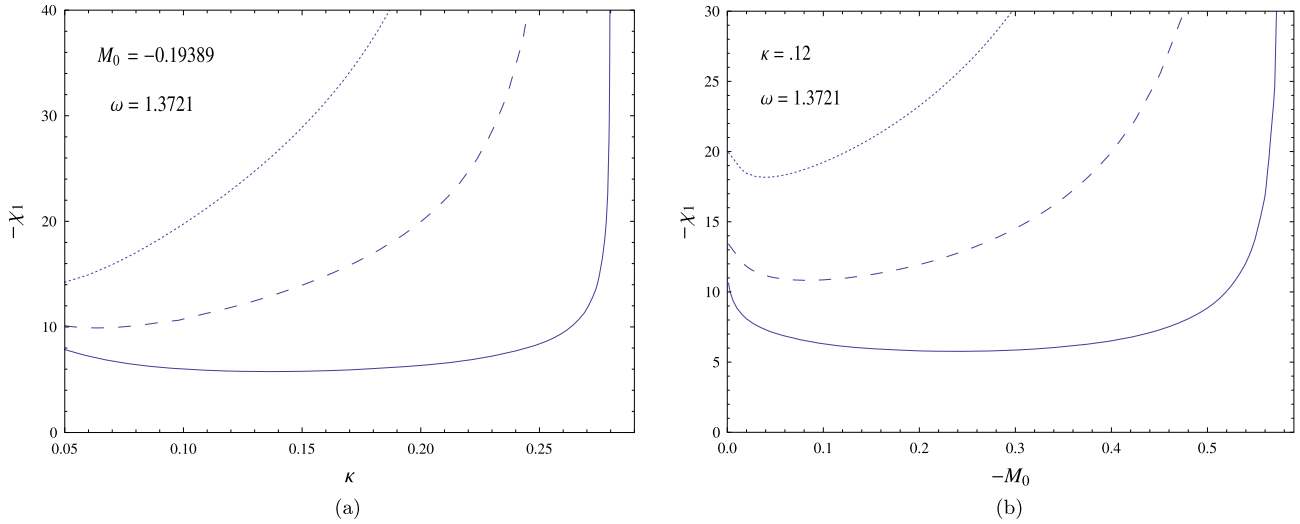

Fig. 8. In (a), $-\chi_1(\kappa)$ [with $\omega \approx 1.3721$ and $M_0 \approx -.019389$] is plotted for the solutions having monotonically decreasing χ (solid curve), the single node solutions (dashed curve) and the double node solutions (dotted curve). The maximum value for κ for the zero node solutions is approximately .28. In (b), $-\chi_1(-M_0)$ [with $\omega \approx 1.3721$ and $\kappa \approx .12$] is plotted for the solutions having monotonically decreasing χ (solid curve), the single node solutions (dashed curve) and the double node solutions (dotted curve). The maximum value for $-M_0$ for the zero node solutions is approximately .58.

$$\{e^{i\psi}, \mathcal{J}\} = ie^{i\psi} \,. \tag{17}$$

In passing to the quantum theory the spectrum of the operator $\hat{\mathcal{J}}$ corresponding to $\mathcal{J}$ is not unique, the eigenvalues being integers plus an arbitrary constant [30,31]. It obeys the commutator

$$[\widehat{e^{i\psi}}, \hat{\mathcal{J}}] = -\hbar\, \widehat{e^{i\psi}} \,, \tag{18}$$

where $\widehat{e^{i\psi}}$ is the operator corresponding to $e^{i\psi}$. The algebra has the Casimir operator $\exp \frac{2\pi i}{\hbar}\hat{\mathcal{J}}$, whose eigenvalues are phases $e^{i\phi_0}$ which label different irreducible representations in the quantum theory. The spectrum for $\hat{\mathcal{J}}$ is then $\hbar$ times an integer m plus an arbitrary phase constant, $\hbar m + \frac{\phi_0 \hbar}{2\pi}$, and so from (16) the energy eigenvalues are

$$E_m = \frac{\hbar^2}{2\mathcal{I}}\Big(m + \frac{\phi_0}{2\pi}\Big)^2 + \mathcal{M} \tag{19}$$

Of course the energy spectrum depends on an additional integer n, the winding number, since $\mathcal{I}$ and $\mathcal{M}$ do.

5. The question of hairy BTZ black hole solutions

The functions $A(x)$ and $B(x)$ were positive for all of the numerical solutions obtained previously by integrating either from $x \to 0$ or $x \to \infty$. Thus none of these solutions developed horizons. We can instead try to a priori assume the existence of at least one horizon. In the case of multiple horizons, let $x_H > 0$ denote the location of the outer most one. Then $A(x_H) = 0$. A consistent solution of (8) near the horizon, $|x - x_H| << 1$, can be obtained by demanding that $\tilde{\Omega}(x_H) = -\tilde{\omega}$. A power series expansion for the functions A, B, $\tilde{\Omega}$ and χ can then be determined from three independent parameters, say $B_H = B(x_H)$, $\chi_H = \chi(x_H)$ and $\tilde{\Omega}_1 = \tilde{\Omega}'(x_H)$, as well as x_H. Up to first order in $x - x_H$,

$$\begin{aligned}
A &\to A_1\,(x - x_H) + \mathcal{O}\Big((x - x_H)^2\Big) \\
B &\to B_H + B_1\,(x - x_H) + \mathcal{O}\Big((x - x_H)^2\Big) \\
\tilde{\Omega} &\to -\tilde{\omega} + \tilde{\Omega}_1\,(x - x_H) + \mathcal{O}\Big((x - x_H)^2\Big) \\
\chi &\to \chi_H + \chi_1\,(x - x_H) + \mathcal{O}\Big((x - x_H)^2\Big) \,,
\end{aligned} \tag{20}$$

where the horizon parameters A_1, B_H, B_1, $\tilde{\Omega}_1$, χ_H and χ_1 satisfy

$$\begin{aligned}
A_1 &= 2B_H x_H - \frac{\tilde{\Omega}_1^2 x_H^3}{2} - \frac{\kappa B_H \sin^2\chi_H}{x_H} \\
B_1 &= 2\kappa x_H B_H\Big(\chi_1^2 + \frac{B_H \tilde{\Omega}_1^2 \sin^2\chi_H}{A_1^2}\Big) \\
\chi_1 &= \frac{B_H \sin(2\chi_H)}{2x_H^2 A_1} \,.
\end{aligned} \tag{21}$$

Setting χ at $x = x_H$ equal to an integer multiple of π in (21) leads to $\chi_1 = 0$, along with the vanishing of higher derivatives of χ at $x = x_H$. Therefore, there are no solutions with $\chi(x_H) = n\pi$, and so the domain $x \geq x_H$ of the nonlinear σ-model cannot be taken to be S^2. Since we desire no horizons in the domain $x \geq x_H$, we require that $A(x), B(x) > 0$ in this domain and so $A_1 > 0$. It follows from (21) that $B_H(1 - \frac{\kappa \sin^2\chi_H}{2x_H^2}) > \frac{\tilde{\Omega}_1^2 x_H^2}{4}$ and $\sin^2\chi_H < \frac{2x_H^2}{\kappa}$.

The above conditions are of course satisfied for the 'bald' BTZ solution where the four functions A, B, $\tilde{\Omega}$ and χ are respectively

$$\begin{aligned}
&A_{BTZ} = x^2 - M + \frac{J^2}{x^2} \qquad B_{BTZ} = 1 \qquad \tilde{\Omega}_{BTZ} = \tilde{\Omega}_\infty + \frac{J}{x^2} \\
&\chi_{BTZ} = 0 \,.
\end{aligned} \tag{22}$$

Then identifying x_H with the outer horizon, $x_H^2 = \frac{1}{2}\big(M + \sqrt{M^2 - 4J^2}\big)$, we get the following results for the horizon parameters

$$\begin{aligned}
&A_1 = \frac{2}{x_H}\sqrt{M^2 - 4J^2} \qquad B_H = 1 \qquad \tilde{\Omega}_1 = -\frac{2J}{x_H^3} \\
&\tilde{\Omega}_\infty + \tilde{\omega} + \frac{J}{x_H^2} = B_1 = \chi_H = \chi_1 = 0 \,,
\end{aligned} \tag{23}$$

which satisfy (21).

For a hairy black hole we drop the restriction of $\chi_H = \chi_1 = 0$ as well as the other results in (23) that follow for the BTZ solution. A monotonically decreasing function $\chi(x)$ and monotonically increasing function for $A(x)$ require $\chi_1 < 0$ and $A_1 > 0$, respectively. From the last equation in (21) and $B_H > 0$ it follows that $\sin(2\chi_H) < 0$. Given these inequalities on the horizon parameters,

along with the conditions (21), we can then integrate the equations of motion (8) from x_H to $x \to \infty$. Upon so doing we were unable to recover the asymptotic solution (9) at $x \to \infty$, and hence we did not find any black hole solutions with nonlinear σ-model hair.

6. Concluding remarks

We obtained numerical solutions for two types, *i*) and *ii*), of rotating self-gravitating topological solitons of the nonlinear σ-model where the space–time approaches AdS^3 in the large distance limit. Upon embedding the solutions in $3+1$ dimensions, they can be interpreted as cosmic strings. For the type *i*) solution, any time slice of the space–time domain has a causal singularity, which is analogous to the BTZ black hole singularity. On the other hand, the space–time domain is singularity free for type *ii*) solutions. $\chi(x)$ for such solutions exhibits an arbitrary number of nodes. No evidence of a horizon was seen for any of the solutions. Therefore these solutions are not hairy black holes, and furthermore the type *i*) solutions have naked singularities.

Among the lines of inquiry that remain to be investigated is the search for black hole solutions with nonlinear σ-model hair, analogous to the known $3+1$ dimensional black hole solutions with Skyrme hair. This may require the inclusion of higher order derivative terms, analogous to the Skyrme term, in the nonlinear σ-model action. While the solitons obtained here are topologically stable, the question of whether or not they are stable under local fluctuations needs to be determined. Finally, it is worthwhile to understand the role that these new three-dimensional AdS solutions may or may not play for the two-dimensional space–time boundary field theory.

References

[1] E. Witten, Anti-de Sitter space, thermal phase transition, and confinement in gauge theories, Adv. Theor. Math. Phys. 2 (1998) 505.

[2] M. Banados, C. Teitelboim, J. Zanelli, The black hole in three-dimensional space–time, Phys. Rev. Lett. 69 (1992) 1849, http://dx.doi.org/10.1103/PhysRevLett.69.1849;
M. Banados, M. Henneaux, C. Teitelboim, J. Zanelli, Geometry of the $(2+1)$ black hole, Phys. Rev. D 48 (1993) 1506, Erratum: Phys. Rev. D 88 (2013) 069902.

[3] G.T. Horowitz, R.C. Myers, The AdS/CFT correspondence and a new positive energy conjecture for general relativity, Phys. Rev. D 59 (1998) 026005.

[4] M. Henneaux, C. Martinez, R. Troncoso, J. Zanelli, Black holes and asymptotics of $2+1$ gravity coupled to a scalar field, Phys. Rev. D 65 (2002) 104007.

[5] M. Banados, S. Theisen, Scale invariant hairy black holes, Phys. Rev. D 72 (2005) 064019.

[6] Y. Brihaye, B. Hartmann, S. Tojiev, AdS solitons with conformal scalar hair, Phys. Rev. D 88 (2013) 104006.

[7] A. Anabalon, D. Astefanesei, D. Choque, Hairy AdS solitons, arXiv:1606.07870 [hep-th].

[8] P. Bizon, A. Wasserman, A note on the non-existence of sigma-model solitons in the $2+1$ dimensional AdS gravity, Phys. Rev. D 71 (2005) 108701.

[9] G. Clement, Field-theoretic extended particles in two space dimensions, Nucl. Phys. B 114 (1976) 437.

[10] M. Heusler, S. Droz, N. Straumann, New black hole solutions with hair, Phys. Lett. B 268 (1991) 371;
Stability analysis of selfgravitating skyrmions, Phys. Lett. B 271 (1991) 61;
M. Heusler, N. Straumann, Z.h. Zhou, Selfgravitating solutions of the Skyrme model and their stability, Helv. Phys. Acta 66 (1993) 614.

[11] T. Ioannidou, B. Kleihaus, J. Kunz, Spinning gravitating skyrmions, Phys. Lett. B 643 (2006) 213.

[12] N.K. Glendenning, T. Kodama, F.R. Klinkhamer, Skyrme topological soliton coupled to gravity, Phys. Rev. D 38 (1988) 3226.

[13] B.M.A.G. Piette, G.I. Probert, Towards skyrmion stars: large baryon configurations in the Einstein–Skyrme model, Phys. Rev. D 75 (2007) 125023.

[14] S. Nelmes, B.M.A.G. Piette, Skyrmion stars and the multilayered rational map ansatz, Phys. Rev. D 84 (2011) 085017.

[15] H. Luckock, I. Moss, Black holes have skyrmion hair, Phys. Lett. B 176 (1986) 341.

[16] P. Bizon, T. Chmaj, Gravitating skyrmions, Phys. Lett. B 297 (1992) 55;
Critical collapse of skyrmions, Phys. Rev. D 58 (1998) 041501.

[17] B. Kleihaus, J. Kunz, A. Sood, SU(3) Einstein–Skyrme solitons and black holes, Phys. Lett. B 352 (1995) 247.

[18] T. Tamaki, K.i. Maeda, T. Torii, Internal structure of Skyrme black hole, Phys. Rev. D 64 (2001) 084019.

[19] N. Sawado, N. Shiiki, K.i. Maeda, T. Torii, Regular and black hole skyrmions with axisymmetry, Gen. Relativ. Gravit. 36 (2004) 1361;
N. Shiiki, N. Sawado, Regular and black hole solutions in the Einstein–Skyrme theory with negative cosmological constant, Class. Quantum Gravity 22 (2005) 3561;
Black hole skyrmions with negative cosmological constant, Phys. Rev. D 71 (2005) 104031;
Black holes with Skyrme hair, arXiv:gr-qc/0501025.

[20] Y. Brihaye, T. Delsate, Skyrmion and Skyrme-black holes in de Sitter spacetime, Mod. Phys. Lett. A 21 (2006) 2043.

[21] A.B. Nielsen, Skyrme black holes in the isolated horizons formalism, Phys. Rev. D 74 (2006) 044038.

[22] Y.S. Duan, X.H. Zhang, L. Zhao, Topological aspect of black hole with Skyrme hair, Int. J. Mod. Phys. A 21 (2006) 5895.

[23] D.D. Doneva, I.Z. Stefanov, S.S. Yazadjiev, Solitons and black holes in a generalized Skyrme model with dilaton-quarkonium field, Phys. Rev. D 83 (2011) 124007;
D.D. Doneva, K.D. Kokkotas, I.Z. Stefanov, S.S. Yazadjiev, Time evolution of the radial perturbations and linear stability of solitons and black holes in a generalized Skyrme model, Phys. Rev. D 84 (2011) 084021.

[24] G.W. Gibbons, C.M. Warnick, W.W. Wong, Non-existence of skyrmion–skyrmion and skrymion–anti-skyrmion static equilibria, J. Math. Phys. 52 (2011) 012905.

[25] F. Canfora, H. Maeda, Hedgehog ansatz and its generalization for self-gravitating skyrmions, Phys. Rev. D 87 (2013) 084049.

[26] G. Dvali, A. Gussmann, Skyrmion black hole hair: conservation of baryon number by black holes and observable manifestations, arXiv:1605.00543 [hep-th].

[27] C. Adam, O. Kichakova, Y. Shnir, A. Wereszczynski, Hairy black holes in the general Skyrme model, Phys. Rev. D 94 (2016) 024060.

[28] S.B. Gudnason, M. Nitta, N. Sawado, Black hole skyrmion in a generalized Skyrme model, arXiv:1605.07954 [hep-th].

[29] J.W. York Jr., Role of conformal three geometry in the dynamics of gravitation, Phys. Rev. Lett. 28 (1972) 1082;
G.W. Gibbons, S.W. Hawking, Action integrals and partition functions in quantum gravity, Phys. Rev. D 15 (1977) 2752.

[30] M.J. Bowick, D. Karabali, L.C.R. Wijewardhana, Fractional spin via canonical quantization of the O(3) nonlinear sigma model, Nucl. Phys. B 271 (1986) 417.

[31] A.P. Balachandran, G. Marmo, B.S. Skagerstam, A. Stern, Classical Topology and Quantum States, World Scientific, Singapore, 1991, 35 pp.

[32] A. Stern, Frozen solitons in a two-dimensional ferromagnet, Phys. Rev. Lett. 59 (1987) 1506.